Electrostatic Interactions Between FeS Clusters in NADH:Ubiquinone Oxidoreductase (Complex I) from Escherichia coli[†]

Liliya Euro, Dmitry A. Bloch, Mårten Wikström, Michael I. Verkhovsky, and Marina Verkhovskaya*

Helsinki Bioenergetics Group, Institute of Biotechnology, P.O. Box 65, (Viikinkaari 1) 00014 University of Helsinki, Helsinki, Finland

Received October 15, 2007; Revised Manuscript Received December 20, 2007

ABSTRACT: The redox properties of the cofactors of NADH:ubiquinone oxidoreductase (complex I) from *Escherichia coli* were studied by following the changes in electron paramagnetic resonance (EPR) and optical spectra upon electrochemical redox titration of the purified protein. At neutral pH, the FMN cofactor had a midpoint redox potential (E_m) ~ −350 mV ($n = 2$). Binuclear FeS clusters were well-characterized: N1a was titrated with a single ($n = 1$) transition, and $E_m = -235$ mV. In contrast, the titration of N1b can only be fitted with the sum of at least two one-electron Nernstian curves with E_m values of −245 and −320 mV. The tetranuclear clusters can also be separated into two groups, either having a single, $n = 1$, or more complex redox titration curves. The titration curves of the EPR bands attributed to the tetranuclear clusters N2 ($g = 2.045$ and $g = 1.895$) and N6b ($g = 2.089$ and $g = 1.877$) can be presented by the sum of at least two components, each with $E_m^{app} \sim -200/-300$ mV and −235/−315 mV, respectively. The titration of the signals at $g = 1.956-1.947$ (N3 or N7, $E_m = -315$ mV), $g = 2.022$, and $g = 1.932$ (Nx, −365 mV) and the low temperature signal at $g = 1.929$ (N4 or N5, −330 mV) followed Nernstian $n = 1$ curves. The observed redox titration curves are discussed in terms of intrinsic electrostatic interactions between FeS centers in complex I. A model showing shifts of E_m due to the electrostatic interaction between the centers is presented.

The proton-pumping NADH:ubiquinone oxidoreductase, complex I, of *Escherichia coli* houses nine FeS centers and a single molecule of FMN (reviewed in ref *1*). The electrons from the NADH-reduced FMN are transferred to ubiquinone via a chain of FeS clusters, and this process is coupled to translocation of protons across the membrane. Although complex I has been under study for more than 40 years (*2*), its molecular mechanism is not known, and the step of energy conversion linked to electron transfer is not yet localized. To make further progress, it is necessary to characterize the redox properties of the individual electron carriers in the chain. Titrations of FeS centers of complex I from different sources have been performed using submitochondrial particles (*3, 4*), bacterial membranes (*5–7*), or isolated subunits expressed from plasmids (*7, 8*). The first two systems have the advantage of an intact complex I, but the disadvantage is that the relatively small EPR[1] signals from the FeS centers are overlapped by signals of other FeS-containing proteins in the membrane. The isolated subunits have the advantage of well-detected clear signals; however, the obtained E_m values may differ from those in the intact protein due to possible perturbation of the cluster environment in the isolated subunit. As a result, there is no clear consensus on the E_m values of the FeS clusters of complex I. However, it has been widely accepted that most of the clusters are equipotential with E_m values close to −270 mV (*9, 10*), with two exceptions. One of these is center N2, which has the highest midpoint potential, but where variable results have been reported within the range from −30 (*11*) to −220 mV (*6*). The other is N1a, whose midpoint potential is very uncertain and varies with the source of the enzyme within the range from −150 (*5*) to −400 mV (*8*).

Recently, the structure of the hydrophilic fragment of *Thermus thermophilus* complex I has been resolved, and the position and the distances between the FeS centers have been determined (*12*). It became clear that the clusters N3, N4, N5, N6a, N6b, and N2 form a chain, while N1a and N7 are located outside that chain. Taking into account the distances between the centers in the chain (10.7−16.9 Å) and assuming that the dielectric constant inside the protein has a typical value of ≤20, one may predict that there should be electrostatically induced negative cooperativity between the centers.

In the present study, we undertook potentiometric redox titrations of purified complex I from *E. coli* by means of EPR and optical spectroscopy. One-electron Nernstian E_m values for one high-potential (−235 mV; center N1a) and one low-potential center (−365 mV; as yet uncertain identity, Nx) were determined. The centers N1b, N2, and N6b showed more complicated titration curves. We discuss the results on

[†] This work was supported by Biocentrum Helsinki, the Sigrid Jusélius Foundation, the Academy of Finland (Project numbers 200726, 44895, and 115108), and the Helsinki Graduate School in Biotechnology and Molecular Biology (L.E.).

* To whom correspondence should be addressed. Tel: +358-9-191 59749. Fax: +358-9-191 59920. E-mail: Marina.Verkhovskaya@Helsinki.Fi.

[1] Abbreviations: EPR, electron paramagnetic resonance; SHE, standard hydrogen electrode; E_h, applied redox potential vs SHE; E_m, midpoint redox potential vs SHE; LB, Luria broth medium.

10.1021/bi702063t CCC: $40.75
Published on Web 02/13/2008

the basis of electrostatic interactions between FeS clusters in the chain and illustrate these interactions with a model.

EXPERIMENTAL PROCEDURES

Bacterial Growth and Purification of Complex I. The *E. coli* MWC215 (Sm^R *nhd*::Cm^R) strain lacking NADH: ubiquinone oxidoreductase II (*13*) was used. Bacteria were grown in LB medium at 37 °C in a 25 L fermentor and harvested at the second half of the exponential phase of growth. The membranes were obtained by passing the cells through an APV Gaulin homogenizer as in ref *14*. Complex I was purified by two chromatography steps, using two anion exchanger DEAE-Trisacryl M (Bio-Sepra) columns, followed by purification on sucrose density gradient as described in ref *15*.

Activation of Complex I for Redox Titrations. Because taking the EPR redox curve required several days with alternate freezing and thawing of the sample, it was necessary to obtain good stability of the protein, which was ascertained by complex I activation with phospholipids. Purified complex I was activated by mixing with asolectin (soybean phospholipids, l-α-phosphatidylcholine, type II-S, Sigma) as described in ref *14*.

Redox Titration by EPR. EPR spectroelectrochemical redox titrations were accomplished using a titrator designed by Harder et al. (*16, 17*) with some modifications. A quartz tube (OD 5 mm, ID 4 mm, length 170 mm) was attached to a quartz-to-glass graded seal and then to an all-glass electrochemical compartment. The latter contained a ST7/15 male joint for degassing/gas purging, which also served for anaerobic loading of the sample, making additions, and cleaning the cell. A ST14/24 male joint connected the EC compartment with the head, which contained all of the electrodes including a wire to the gold working electrode. The electrochemical cell utilized a typical three-electrode circuit with saturated Ag/AgCl reference, Pt foil counter electrodes, and a gold (99.99%) foil working electrode. The reference and counter electrodes were connected through a Vycor fret (1 kOhm) and a 3 M KCl bridge filled with anaerobic KCl. The setup permitted convenient transfer of the sample between the electrochemical compartment and the EPR tube by a simple rotation of the cell; thus, oxygen leakage that would disturb the ambient potential during sample transfer was avoided. A buffer (400 μL) was degassed by cycling with vacuum and He (99.9999%) for at least 3 h, and then, the traces of oxygen (e.g., leaking in from the fret) were quenched electrochemically by poising the potential at −400 mV. Under a high positive gas flow, buffer was removed and sample (400 μL) in anaerobic buffer was added to the cell with a 1 mL syringe (gastight, Hamilton). The sample of 400–500 μL, containing 4–7 mg/mL of activated complex I in the buffer consisting of 66 mM NaCl, 1.5% (w/v) glycerol, 6% (w/v) sucrose, 0.05% *n*-dodecyl β-D-maltoside, 0.18% (w/v) sodium cholate, 18 mg/mL asolectin, 33 mM MES/NaOH, and 66 mM HEPES/KOH, pH 7.0, and mediators [methylviologen 50 μM (E_m = −455 mV), benzylviologen 50 μM (E_m = −360 mV), hexaammineruthenium 200 μM (E_m = 50 mV), and pentaamminechlororuthenium 400 μM (E_m = −130 mV)], was degassed by cycling with vacuum and He; then, the traces of oxygen were quenched electrochemically by poising the potential at −400 mV. A potentiostat PAR263A (Princeton Applied Research) was employed to poise the potential below the desired equilibrium potential. Subsequently, the potentiostat was turned off, and the solution was allowed to drift to equilibrium while a voltmeter across the working and reference electrodes measured the ambient potential. When equilibrium had been achieved, as evidenced by a significant decrease followed by stabilization of the electrical current through the cell, the cell was tipped to transfer the solution to the EPR tube; the solution was then transferred back to the electrochemical compartment, and the potential was recorded. The sample was then retransferred to the EPR tube and immediately frozen in liquid nitrogen for EPR spectroscopy. This cycle was repeated to obtain a titration curve. Titrations were performed in both oxidative and reductive directions, and no significant hysteresis was detected, indicating that equilibration with mediators was adequate. The data shown represent the combined results of four independent titrations taken in different directions.

EPR Spectroscopy. X-band (9.4 GHz) EPR measurements were performed with a Bruker EMX EPR spectrometer equipped with an Oxford Instruments ESR900 helium flow cryostat with an ITC4 temperature controller. The field modulation frequency was 100 kHz, and the modulation amplitude was 1.27 mT. The microwave power incident to the cavity and the sample temperature are indicated in the figures. Because no redox changes in complex I are known at redox potentials higher than −100 mV, the EPR spectra around this point were used as a baseline. The spectral simulation was performed using software WinEPR SimFonia Version 1.26 (beta). (Bruker Analytic GmbH). The spin quantification was based on double integration of simulated individual signals with the peak amplitude equal to that in unsaturated spectra. Some data on microwave power and temperature dependence are included in the Supporting Information (Figures 2−4).

Optical Redox Titration. Spectroelectrochemical redox titration of complex I was done at 21 °C using the OTTLE cell as described in ref *18*. The potential within the range from −500 to −40 mV was applied with ±20 mV steps during both oxidative and reductive titrations using a PAR263A potentiostat (Princeton Applied Research). Optical absorption spectra were recorded in the spectral range of 350–750 nm with absorption at 700 nm as a reference. At each potential step, the onset of equilibrium on the working electrode was determined as the point where changes in optical absorption at 450 nm were no longer significant. To accelerate the redox equilibrium between the working electrode and the solubilized enzyme, the redox mediators were added as follows: hexaammineruthenium, 200 μM; pentaammineruthenium, 400 μM; methyl viologen, 50 μM; and cobalt(III) sepulchrate (E_m = −350 mV), 100 μM. No optical contribution from hexaammineruthenium, pentaammineruthenium (ABCR GmbH & Co.), or cobalt sepulchrate was detected in the studied spectral range. The contribution from methyl viologen at potentials below −350 mV was taken into account during the data analysis. For the redox titration, 60 μL of solution of complex I, 40 mg/mL in 70 mM HEPES/KOH (pH 7.5), 67 mM NaCl, 7% (w/v) sucrose, 1.5% (w/v) glycerol, 0.1% *n*-dodecyl β-D-maltoside, 20 mg/mL asolectin, and 0.18% (w/v) sodium cholate with added mediators, was degassed on a vacuum line and flushed

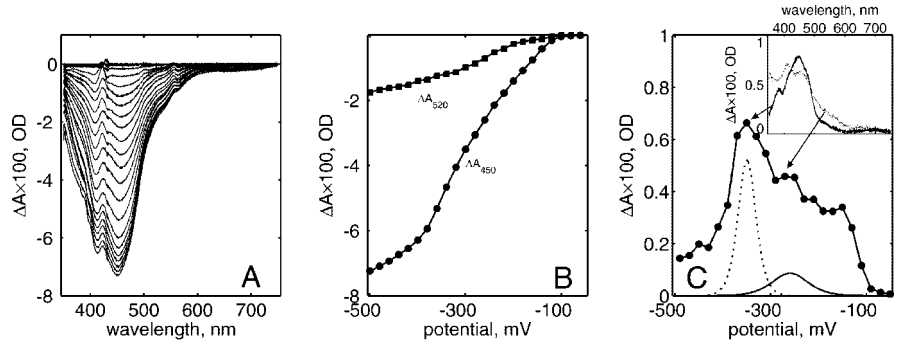

FIGURE 1: Optical redox titration of complex I. (A) Redox spectra of complex I obtained at redox potentials from −500 to −40 mV with step 20 mV. (B) Titration curves at 450 and 520 nm. (C) The derivative of the titration curve at 450 nm from the set of difference spectra (obtained by subtraction of spectra with adjacent potentials). Theoretical two-electron (dotted line) and one-electron (solid line) curves correspond to titration of flavin (ϵ_{450} = 12800 M^{-1} cm^{-1}) and FeS centers (ϵ_{450} = 4100 M^{-1} cm^{-1}), respectively. Inset: difference spectra for −340 minus −360 mV (solid line) and −260 minus −280 mV (dotted line). Arrows specify at which points spectra were obtained.

with argon 10 times. Finally, the protein mixture was anaerobically loaded into the OTTLE cell (0.6 mm optical path length) that was also degassed and filled with argon. The titrations were performed in both the oxidative and the reductive directions without noticeable hysteresis.

RESULTS

Redox Titration of Complex I by Optical Spectroscopy. The data on spectroelectrochemical redox titration of complex I are presented on Figure 1. The spectra reflect oxidoreduction of the FMN cofactor and all FeS centers in the protein (Figure 1A). The redox spectra of the iron sulfur clusters have relatively low extinction; their absorbance bands are broad and similar to one another. Therefore, these spectra are difficult to decompose into individual components. However, by comparison of the titration curves (Figure 1B) at 450 nm where all redox centers have some absorbance and at 520 nm where the flavin cofactor does not contribute (*19*), we could determine the midpoint potential of FMN, which apart from ubiquinone is the only two-electron carrier in complex I, and has an extinction coefficient at 450 nm (*20*), which is about three times larger than individual extinction coefficients of binuclear (*21*) and tetranuclear (*22*) FeS centers. The titration curve at 450 nm shows a component with a maximal slope in the range of −340 to −360 mV. The derivative of the titration curve at 450 nm [Figure 1C (●)] demonstrates a sharp (n = 2) peak at −350 mV that overlaps an underlying broadband, reflecting superposition of peaks from all FeS centers with different midpoint potentials. For illustration, two theoretical curves are shown in Figure 1C: for a two-electron acceptor (E_m = −350 mV) with extinction coefficient 12.8 mM^{-1} cm^{-1} (dashed line) (*19*) and for a one-electron acceptor (E_m = −270 mV) with the extinction coefficient 4.1 mM^{-1} cm^{-1} (solid line) (*21, 22*). The two difference spectra, −340 minus −360 mV and −260 minus −280 mV (Figure 1C, inset), clearly demonstrate that the major part of the redox changes derives from FMN in the first case and from FeS clusters in the second.

The region of the spectrum where the FeS centers absorb but FMN does not, that is, above 500 nm, shows monotonic absorption increases from −100 to −500 mV [Figure 1B (■)]. This demonstrates that there are no equipotential FeS centers, which, if present, should produce Nernstian n = 1 curves with a common E_m. The slightly larger slope at −270 mV shows that a larger number of FeS centers have midpoint potentials in this area. Altogether, as better seen in Figure 1C, all midpoint potentials of FeS clusters are dispersed between −160 and −500 mV.

Redox Titration of Binuclear FeS Centers by EPR Spectroscopy. The EPR spectrum of complex I is complicated, consisting of up to nine overlapping individual signals. To simplify the system, we used selective temperature and microwave power conditions. At a sample temperature of 45 K and 2 mW microwave power, only binuclear clusters contribute to the EPR spectrum (Figure 2, upper panel). This spectrum is composed of two signals only, viz. those of N1a and N1b, and can be easily simulated by their individual spectra shown in the inset. The parameters of the simulated N1a, g_{xyz} = 1.92, 1.95, and 2.00, and N1b, g_{xyz} = 1.930, 1.938, and 2.021, spectra are in good agreement with literature data (*23, 24* and *6, 7, 25*, respectively). The spectra of the binuclear centers were deconvoluted at each redox potential with individual signals, and the dependence of the spin concentration on redox potential is presented in Figure 2. The N1a cluster behaved as a pure one-electron carrier with a midpoint potential of −235 mV (middle panel). In contrast, the slope of the titration curve of N1b (lower panel) was smaller than that for a single one-electron component, as shown in the figure.

Redox Titration of Tetranuclear FeS Centers of Complex I by EPR Spectroscopy. At a temperature of 10 K and microwave power higher than 0.2 mW, the binuclear centers are mostly saturated and their contribution to the spectrum is small. However, the spectrum at these conditions is still too complicated for decomposition. Using difference spectra at the high- and low-potential edges of the titration range, we could resolve individual signals of two FeS clusters (Figure 3). The difference between the spectra at −171 and −118 mV gives a clear signal of a single axial FeS cluster. The parameters of this signal, g_{xyz} = 1.895, 1.904, and 2.045, coincide with that of the N2 spectrum simulated earlier (*14, 15*), which therefore represents the highest potential feature among the tetranuclear centers. The resolved center with the lowest potential is also dominated by an axial type signal with the parameters g_{xyz} = 1.931, 1.935, and 2.022. This signal has not been described earlier, presumably because it is relatively small in amplitude and overlaps with the N1b signal in the spectrum of complex I reduced by NADH. Despite the similarity of spectra, this signal hardly

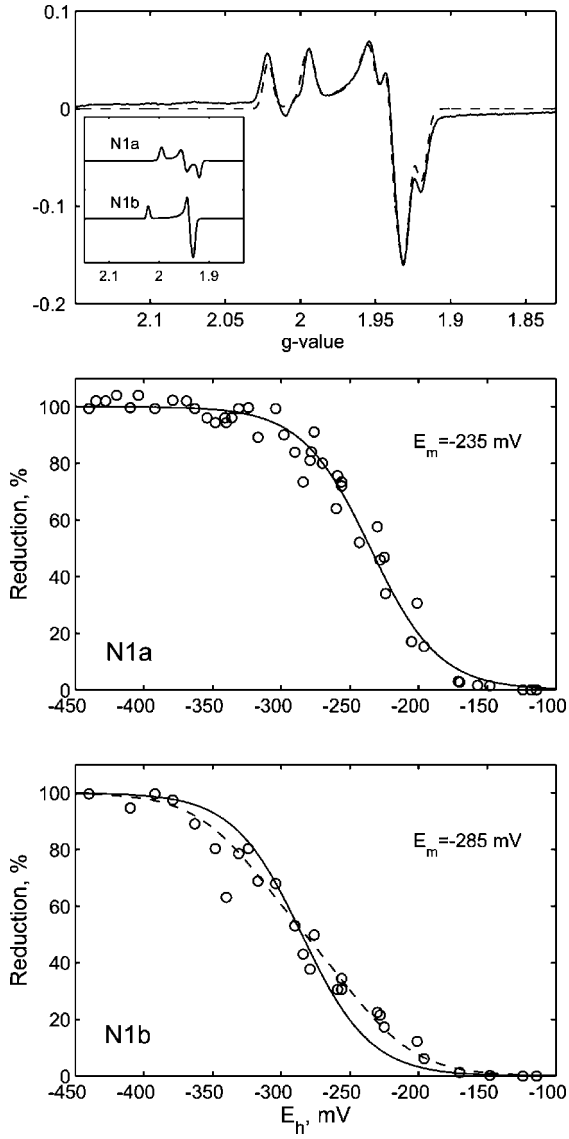

FIGURE 2: Redox titration of binuclear FeS clusters of complex I. Upper panel: EPR spectra at −400 mV; sample temperature, 45 K; microwave power, 2 mW. The spectrum consists of two individual signals derived from N1a and N1b. The simulation of these signals with parameters g_{xyz} = 1.92, 1.95, and 2.00 (N1a) and g_{xyz} = 1.930, 1.938, and 2.021 (N1b) is shown in the inset. The experimental spectrum can be fitted with the sum of simulated N1a and N1b signals in the proportion 1:0.86 (dashed line). Middle panel: The titration of the N1a signal amplitude (circles) takes the shape of a one-electron redox curve with E_m = −235 mV (solid line). Lower panel: The titration of the N1b signal amplitude (circles) cannot be fitted with a single one-electron redox curve (E_m = −285 mV, solid line) but fits to the sum of two one-electron redox curves with E_m = −245 and −320 mV in the ratio 1:1 (dashed line).

derives from N1b. Titration of the g = 1.93 band yielded redox curves that were different in shape and E_m at 45 and 10 K, suggesting contribution from more than one cluster because the redox properties should not depend on measurement conditions. Also, the saturation properties of the g = 1.93 band changed more at low than at high temperature upon reduction (see Figure 2, Supporting Information). The nature of this signal is discussed further below; for the time being, we call it Nx.

Because of the complexity of the spectra in the middle redox titration potential range (see the example of raw data in Figure 1, Supporting Information), it was not possible to unequivocally decompose the data into spectra of individual centers. Therefore, the most prominent features, peaks, and troughs that belong to known centers were used for the titration (Figure 4). The N2 and N6b spectra were simulated previously (*14, 15*), and the spectrum of Nx was simulated from the low-potential component of the complex I titration (Figure 3, lower panel). The spectrum of the N3 (or N7) cluster was simulated on the basis of literature data.

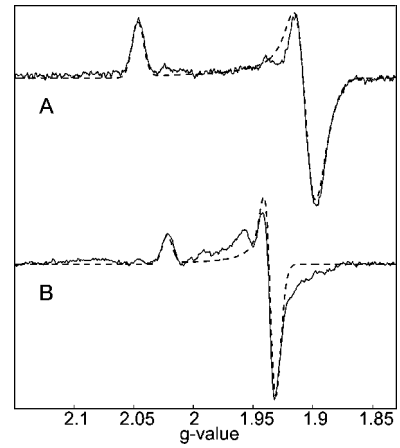

FIGURE 3: Resolved individual spectra of tetranuclear FeS clusters with the highest and lowest midpoint potential. The EPR spectra obtained from different redox transitions taken at 10 K: 10 (A) and 2 mW (B). (A) The "−171 mV" minus "−118 mV" difference spectrum corresponds to the spectrum of N2 (g_{xyz} = 1.895, 1.904, and 2.045). (B) The "−435 mV" minus "−369 mV" difference spectrum temporarily assigned as Nx can be simulated with parameters g_{xyz} = 1.931, 1.935, and 2.022.

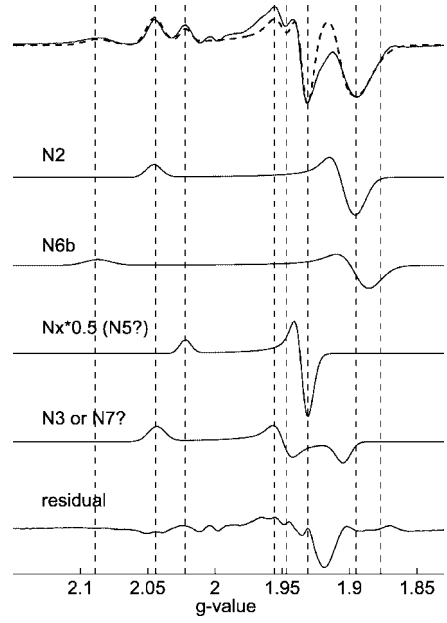

FIGURE 4: Determination of characteristic points in the EPR spectrum of complex I for plotting the titration curves of [4Fe-4S] centers. Upper line, the spectrum of reduced complex I (E_h = −410 mV) taken at 10 K and 2 mW (solid line). The simulated spectra of four major components, N2, N6b, Nx, and N3 (N7), are shown below; their sum in the proportion 1:1:0.5:1 overlays the experimentally obtained spectrum of complex I (dashed line). The difference between the experimental spectrum and the sum of simulated spectra is shown at the bottom. The characteristic points were taken at g = 2.045 and 1.895 for N2, g = 2.089 and 1.877 for N6b, and g = 2.022 and 1.932 for Nx and the difference between g = 1.956 and g = 1.947 for N3.

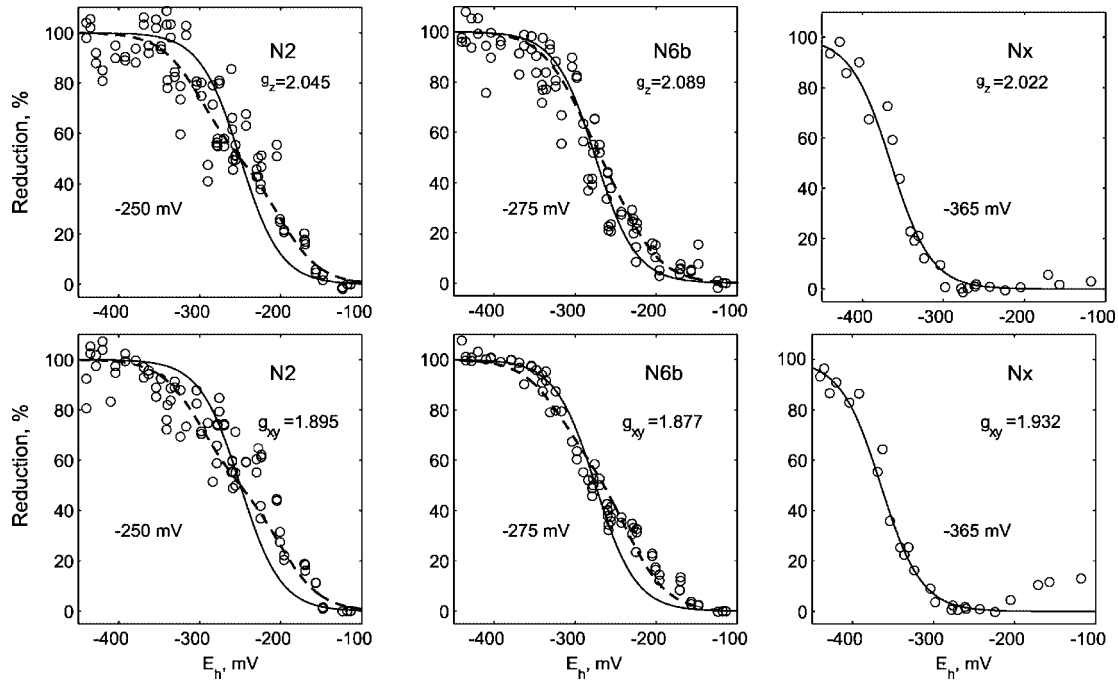

FIGURE 5: Redox titration of clusters N2, N6b, and Nx. The titration of signal amplitude at the characteristic points for g_z (upper row) and g_{xy} (lower row) of clusters N2, N6b, and Nx (circles). The data were obtained at 10 K and 10 and 2 mW for N2 and N6b clusters and 10 mW for Nx. The one-electron redox curves (solid line) with indicated E_m values are drawn through the experimental points. The titration of the Nx cluster agrees with a one-electron redox curve, but the titration of N2 and N6b is better satisfied by the sum of two one-electron components (N2, $E_m = -200$ and -300 mV, ratio 1:1; N6b, $E_m = -235$ and -315 mV, at g_z, ratio 1:1, and at g_{xy}, ratio 1.5:1) (dashed line).

Parameters of $g_{xyz} = 1.86$, 1.95, and 2.05 (*26*), 1.9, 1.95, and 2.05 (*24*), and 1.88, 1.94, and 2.045 (*6*) have been reported for the N3 cluster. Very similar parameters were published for the N7 cluster; $g_{xyz} = 1.916$, 1.94, and 2.048 (*25*), 1.91, 1.94, and 2.05 (*27*), and 1.894, 1.953, and 2.047 (*28*). The characteristic points of the N2 signal at $g = 2.045$ and $g = 1.895$ were found from the spectrum of the high potential component (Figure 3A) and previous N2 simulations. Because it was suggested that N2 is the main contributor to the resonance at these g values at low temperature and high microwave power, the signal amplitude at $g = 2.045$ and $g = 1.895$ was plotted against redox potential to obtain the titration of N2 (Figure 4). The signal amplitudes at $g = 2.089$ and 1.877 and $g = 2.022$ and 1.932 were used for characterization of the redox properties of N6b (g_z and g_{xy}) and Nx (g_z and g_{xy}), respectively (Figure 4). The characteristic point for N6b was deliberately shifted from the maximal signal at $g = 1.887$ to $g = 1.877$ to minimize N2 contribution. The characteristic points for N3 (N7) were chosen from the part of the spectrum where the signals of other clusters have minimal contribution.

The titration curves for N2 and N6b did not agree with a one-electron redox curve in either the g_z or the g_{xy} areas, and the experimental points can be fitted much better with the sum of at least two one-electron components, as shown in Figure 5. The shape of the titration curves for the N2 and N6b clusters was not dependent on microwave power in the range 2–63 mW; Figure 5 presents the data obtained at 2 and 10 mW. Because the Nx and N1b spectra are very similar, to suppress any contribution of N1b, which is small at low temperature (10 K), we used only the data obtained at high microwave power (10 mW) for plotting the titration curve of Nx. The low potential Nx cluster clearly titrated as a one-electron carrier with $E_m = -365$ mV. The titration of

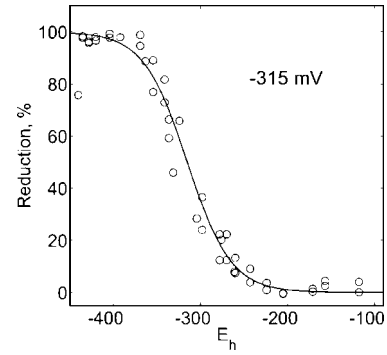

FIGURE 6: Redox titration of cluster N3 (N7). The difference of amplitudes at $g = 1.956$ and 1.947 (see Figure 3) is plotted against the redox potential. The data were obtained at 10 K and 10 and 2 mW. A one-electron redox curve (solid line) with indicated E_m value is drawn through the experimental points.

N3 (N7) also followed a one-electron Nernstian curve with $E_m = -315$ mV (Figure 6).

The EPR spectrum at 5.5 K and 10 mW microwave power deriving from the fastest relaxing clusters has a prominent feature, a trough, at $g = 1.929$ (Figure 7). There is also a wide signal present at $g = 1.8$–1.9 derived from the strongly saturated N2 and N6b clusters and probably from other cluster(s) as well. This broad signal was difficult to analyze, whereas the sharp signal at $g = 1.929$ can be titrated as a single one-electron component with $E_m = -330$ mV (Figure 7). The determined properties of complex I cofactors are summarized in Table 1.

DISCUSSION

The redox properties of electron carriers in complex I provide a thermodynamic basis for the understanding of the

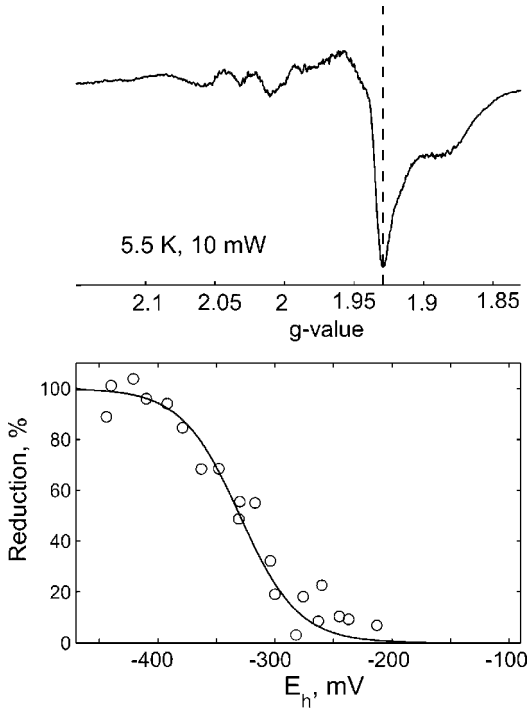

FIGURE 7: Redox titration of the fastest relaxing FeS cluster(s). Upper panel: The spectrum of reduced complex I at 5.5 K and 10 mW. The characteristic point chosen for the titration was at $g = 1.929$. Lower panel: Redox titration of the signal amplitude at 1.929 (circles) can be fitted with a one-electron redox curve with $E_m = -330$ mV.

molecular mechanism of energy transformation by the enzyme. However, few attempts to determine the midpoint potentials of the redox centers in complex I have been undertaken, mainly due to the high complexity of the system. The redox state of FeS centers can be followed by low-temperature EPR measurements, but the EPR spectra of complex I are a combination of overlapping signals from several FeS centers, the individual spectra of which are not completely defined so far. Attributing observed signals to particular clusters is not yet well-established. Moreover, the observed signals from mitochondrial complex I differ significantly from those of the bacterial enzymes in spite of high amino acid sequence similarity of the core subunits and similar content of cofactors. In EPR spectra of complex I from *E. coli*, some signals, such as N1a, are not observed in spectra of the mitochondrial enzyme and vice versa; other signals differ in shape and band position. Therefore, one should not automatically transfer names of EPR signals that were defined for the mitochondrial enzyme to bacterial complex I signals.

Up to now, submitochondrial and sub-bacterial membranes containing iron-sulfur proteins from enzymes other than complex I have generally been used for redox titrations (*3–7*). Purified complex I from mitochondria was used only for the titration of binuclear clusters (*29*), where two components, a major ($E_{m8.0} = -335$ mV) and a minor ($E_{m8.0} > -300$ mV) one, were found by redox titration of the $g = 1.94$ signal.

Here, we have for the first time presented redox titrations of purified complex I from *E. coli*. The resolved spectra of the two binuclear clusters, N1a and N1b, clearly showed different redox properties. N1a behaves as a pure one-electron carrier with $E_m = -235$ mV, which is close to the value of −250 mV obtained for this center upon redox titration of sub-bacterial vesicles from *E. coli* by Leif et al. (the former name of N1a was N1c) (*6*). In contrast, the shape of the N1b titration is distorted from a simple $n = 1$ Nernstian curve but fits the sum of two $n = 1$ components. Because the double integration of simulated spectra of N1a and N1b showed that they are present in almost equimolar proportions and there are no other [2Fe-2S] clusters in the enzyme, the complexity of the N1b titration cannot be explained by spectral contribution of other FeS centers but should rather be attributed to a distortion of the intrinsic property of the cluster by redox interaction with other centers.

The interpretation of the data on [4Fe-4S] clusters is much more complicated, because several clusters may contribute to the signal at particular g-values, e.g. $g_z \sim 2.05$ has been reported for clusters N3, N2, and N7 (*6, 9, 23–25, 27*), and a similar situation is found for the signal around $g = 1.9$ where N2, N6b, N3, and N7 may all participate. Although N2 and N6b are faster relaxing than the other clusters, and at 10 K and high microwave power the signal at the mentioned g values derives mainly from these centers, the contribution of other clusters cannot be completely ruled out. Thus, the titrations at $g = 2.045$ and $g = 1.895$, which we consider as characteristic points for N2, may reflect redox transition of N2 at high and N3 or N7 at low potentials. This explanation was suggested for the titration of the EPR signal at $g = 1.9$ in *E. coli* membranes by Leif et al. (*6*), who observed a titration curve similar to that in Figure 5 (N2, g_{xy}). However, another interpretation of the deviation from a single one-electron titration curve (N1b, N2, and N6) becomes evident from inspection of the resolved atomic structure of the hydrophilic fragment of complex I (*12*). Centers N3, N4, N5, N6a, N6b, and N2 form a chain, with individual center-to-center distances of 12–17 Å. Assuming a dielectric constant of ≤20 inside complex I, typical for the interior of a protein (for discussion on the dielectric constant in proteins see refs *30, 31*), electrostatic interactions between centers must be taken into account. Such an interaction would shift the E_m of neighbor center(s) to more negative values on arrival of an electron to a particular FeS cluster, due to electrostatic repulsion between two equivalent charges. It is obvious that such a shift of E_m in a chain of redox centers would be stronger for the inner redox centers than for the ones at the edges (because of the larger number of neighbors). To illustrate such a system behavior, a model was developed, which shows how the electrostatic interactions could affect the titration. The model includes four one-electron centers with the distances between them taken from the X-ray structure (*12*): N3−N1b, 14.2 Å; N1b−N4, 13.9 Å; and N4–N5, 12.2 Å. Figure 8 shows a scheme of the redox transitions between all equilibrium states of the four redox centers. Zeros and ones indicate oxidized and reduced states of each of these centers, respectively. The equilibrium constant between each state for the redox reaction can be expressed through the midpoint redox potential

$$K_{eq} = e^{(E_h - E_m)/RT}$$

where E_m is the midpoint redox potential, E_h is the ambient redox potential, R is the gas constant, and T is the absolute temperature.

Because of electrostatic repulsion, the reduction of any center becomes more difficult when a neighbor center is

Table 1: Electrochemical and EPR Spectral Properties of the Complex I Cofactors of *E. coli*

redox center	E_m (mV)	the basis of titration profiles	g_{xyz}	temperature (K)	microwave power (mW)
FMN	−350 (n = 2)[a]				
			2Fe-2S[b]		
N1a	−235	simulated spectrum	1.920, 1.950, 2.00	45	2
N1b	−320, −245	simulated spectrum	1.930, 1.938, 2.021		
			4Fe-4S[b]		
N2	−300, −200	1.895, 2.045	1.895, 1.904, 2.045	10	10
N6b	−315, −235	1.877, 2.089	1.887, 1.894, 2.089		2, 10
N3 or N7	−315	1.956 minus 1.947	1.90, 1.947, 2.046		2, 10
Nx	−365	1.932, 2.022	1.931, 1.935, 2.022		10
N4 or N5	−330	1.929		5.5	10

[a] Optical titration. [b] EPR titration.

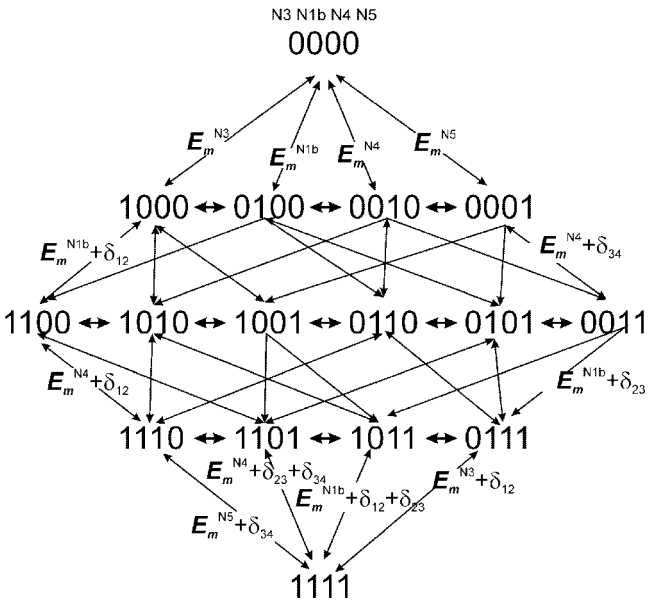

FIGURE 8: Model of redox transitions between all equilibrium states of four redox centers, N3, N1b, N4, and N5. Zeros and ones indicate oxidized and reduced states, respectively. The equilibrium constant between each state of a particular FeS cluster can be expressed through its nominal midpoint redox potential (E_m^{N3}, E_m^{N1b}, E_m^{N4}, and E_m^{N5}) plus the energy of electrostatic repulsion (δ_{12}, δ_{23}, and δ_{34}) when the adjacent FeS cluster(s) is (are) reduced. The δ subscipts indicate the clusters between which the interaction occurs. In accordance with the scheme, N3, N1b, N4, and N5 are denoted 1, 2, 3, and 4, respectively. Examples of equilibrium constants are shown on some of the arrows connecting individual states. Other equilibrium constants can be expressed in similar ways.

reduced, which corresponds to an E_m that is decreased from the starting value by the energy of interaction. The distances between the redox centers allow calculation of the interaction energies if the dielectric constant is known. Assuming that the dielectric constant is 20, the interaction energies are δ_{12} = −50 mV (for the interaction between N3 and N1b), δ_{32} = −51 mV (for the N1b and N4 interaction), and δ_{34} = −59 mV (for the N4 and N5 interaction). Only the interactions between adjacent centers are considered in the model.

During the transition of a system of four redox centers from fully oxidized to fully reduced, the total number of states will be 2^4 = 16 (Figure 8). The equilibrium of electron distribution between fully oxidized (the top state in Figure 8) and one-electron reduced states (Figure 8, second row) is represented by the nominal E_m values of each FeS center, due to the absence of other electrons in neighbor centers. However, for example, reduction of N1b in conditions where N3 and N4 are reduced would have a new apparent E_m = $E_m^{N1b} + \delta_{12} + \delta_{23}$. This approach defines the apparent E_m (or equilibrium constant) for each transition in the scheme and the fraction of each state at any redox potential (the sum of all states at any redox potential is unity). To find the titration profile for any FeS cluster, all states where this center is reduced are summed and plotted against the ambient redox potential. It is important to note that if the E_m of a cluster between two neighbors is, for example, only 60 mV lower than the potential of the neighbors, the apparent E_m for such a cluster will be lower than the E_m of the neighbors by 60 mV plus two interaction energies. This is why the E_m values of some redox centers can be so low that they may not be detectable in the normally used range of redox potentials.

Figure 9 illustrates predictions ensuing from this model. First, if the FeS centers are equipotential, for example, E_m = −270 mV, the observed redox curves could not be fitted by simple n = 1 Nernstian curves but should be shifted to more negative potential and have complex shapes depending on the position in the chain (Figure 9A). Second, the apparent E_m of the middle cluster may be so low that it may be difficult to reduce; this could be a reason for why only four or five [4Fe-4S] clusters out of the seven present in complex I can be observed. An example of such a phenomenon is presented in Figure 9B. The nominal E_m values (without interactions) of clusters N3, N1b, N4, and N5 were set at −285, −265, −350, and −300 mV, respectively, to obtain an N1b titration curve close to the experimental data. As a result of electrostatic interactions, the E_m and the shape of the titration curves were changed. The smallest effect was on clusters N5 and N3 at the edges; the N3 titration curve was indeed close to a one-electron Nernstian, and the midpoint potential was only shifted from −285 to −320 mV. The E_m of cluster N5 did not practically change at all because its E_m is significantly more positive than that for the adjacent cluster N4. N1b, the nominal E_m of which was set at −265 mV, exhibits a complicated titration curve that may be fitted as the sum of two Nernstian n = 1 components with E_m −245 and −320 mV at a ratio of 1:1. The titration curve of the middle N4 cluster with nominal E_m = −350 was much more distorted. It also has two components, but the high-potential component is insignificant and the major low-potential component shows an apparent E_m of less than −450 mV, so negative that it can hardly be approached in the current setup. Indeed, quantitation of our individual spectra of FeS centers in complex I from *E. coli* showed that they are present roughly at the ratio N1a:N1b:N2:N6b:N3(7):Nx = 1:1:1:1:1:0.5, which means that the number of observed spins is significantly lower than nine,

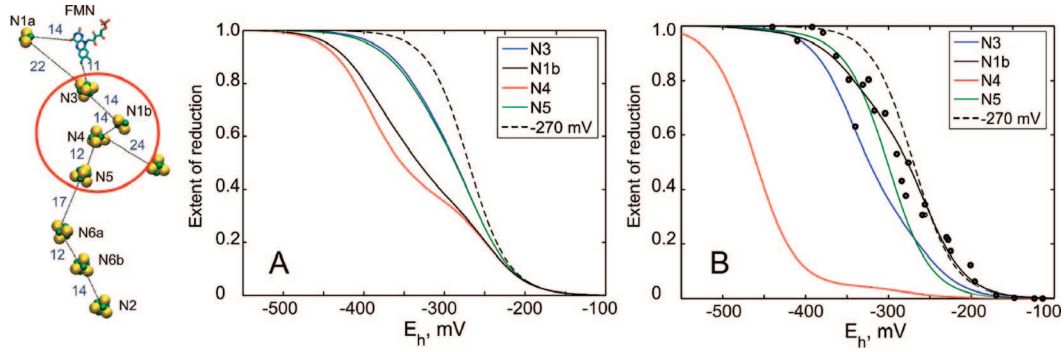

FIGURE 9: Predicted effects of electrostatic interactions between FeS clusters in complex I on the equilibrium redox titration. Left: The structure of FeS clusters in the hydrophilic fragment of complex I (*12*). Four clusters from the chain, N3, N1b, N4, and N5, are considered by the model. The redox curves of these clusters were simulated on the following assumptions. (A) All clusters are equipotential with $E_m = -270$ mV, solid lines; theoretical $n = 1$ Nernstian curve with $E_m = -270$ mV, dashed line. (B) The redox potentials of N3, N1b, N4, and N5 were preset as −285, −265, −350, and −300 mV, respectively, to obtain the N1b titration curve close to the observed data shown by circles. The simulated redox curves are shown by solid lines, theoretical $n = 1$ Nernstian curve with $E_m = -270$ mV, dashed line. The electrostatic interactions between the neighbor centers were calculated from the distance between them with an assumed dielectric constant of 20.

predicted by the structure (*12*). We propose that the rest of the FeS centers are EPR-invisible due to strong electrostatic repulsion from neighbors. It has been shown that the EPR spectra of complex I from mitochondria (*9, 32, 33*) and *E. coli* (*6*) differ significantly, which may be explained not only by possible differences in the individual spectra of analogous redox centers but also because different clusters could be EPR-invisible in complex I from these two sources due to even small differences in redox potentials. As seen from the presented model, small changes in true midpoint potentials of the clusters could yield strong variations in the observed E_m.

On the basis of the above, we may expect that clusters with a redox curve close to $n = 1$ should be either located far from their neighbors or then differ significantly from their neighbors in midpoint redox potential. We found that titration of four FeS clusters can be characterized by simple $n = 1$ curves. One of these is N1a ($E_m = -235$ mV), which is located aside the main chain of FeS clusters and close to FMN. Its interactions with other FeS clusters should be weak but should be appreciable with FMN. However, as determined by the optical titration, the E_m of FMN is −350 mV and should therefore not affect the N1a titration. On the other hand, the very low observed E_m of FMN could itself be a result of electrostatic interactions with the FeS clusters N1a and N3, since they become reduced at higher potentials than FMN. Consequently, the redox potential of FMN may have a significantly more positive value for states where centers N1a and N3 are oxidized. The other center characterized by a simple Nernstian $n = 1$ curve is N3 (or N7) with $E_m = -315$ mV. Because the reported parameters of N3 and N7 are similar (*6, 24–28*) (see above) and both are peripheral in the chain, it is difficult to make a definite assignment. The low-temperature EPR signal at $g = 1.929$ derived from the fastest relaxing cluster also followed a simple $n = 1$ curve ($E_m = -330$ mV). It probably belongs to clusters N4 or N5, since a similar signal was observed in the EPR spectrum of the isolated NuoG subunit (*25*). The amplitude of this signal was low, which could be explained in two ways. Either the cluster may be strongly saturated at low temperature and microwave power or the observed titration may represent only the first wave of a complex titration curve, where the second wave is shifted to a low-potential region beyond the resources of the instrumentation. The last signal that showed a one-electron redox curve derived from a tetranuclear cluster with $g_{xyz} = 1.931$, 1.935, and 2.022 and designated Nx. This low-potential cluster ($E_m = -365$ mV) has a spectrum very similar to N1b but can be resolved from N1b by the difference in saturation and redox properties. It would be logical to assign this cluster to the remote center N7, which does not participate in electron transfer (*28*), but this contradicts the reported parameters of N7 in the EPR spectrum of the isolated NuoG subunit (*25, 27*). Therefore, this signal may alternatively derive from one of the middle clusters in the main chain.

Because of the complexity of the titration data, which is caused by multiple redox interactions and overlapping EPR signals, further studies including site-specific mutagenesis will be required for the detailed analysis of the redox curves and their assignments.

ACKNOWLEDGMENT

We thank Eija Haasanen for growing bacterial cultures and purification of complex I.

SUPPORTING INFORMATION AVAILABLE

EPR spectra of purified complex I and figures of microwave power dependences of the EPR signals. This material is available free of charge via the Internet at http://pubs.acs.org.

REFERENCES

1. Sazanov, L. A. (2007) Respiratory complex I: Mechanistic and structural insights provided by the crystal structure of the hydrophilic domain. *Biochemistry 46*, 2275–2288.
2. Hatefi, Y., Haavik, A. G., and Griffiths, D. E. (1962) Studies on electron transfer system. 40. Preparation and properties of mitochondrial DPNH-coenzyme Q reductase. *J. Biol. Chem. 237*, 1676–1680.
3. Ingledew, W. J., and Ohnishi, T. (1980) An analysis of some thermodynamic properties of iron-sulphur centres in site I of mitochondria. *Biochem. J. 186*, 111–117.
4. Zwicker, K., Galkin, A., Drose, S., Grgic, L., Kerscher, S., and Brandt, U. (2006) The Redox-Bohr group associated with iron-sulfur cluster N2 of complex I. *J. Biol. Chem. 281*, 23013–23017.
5. Meinhardt, S. W., Kula, T., Yagi, T., Lillich, T., and Ohnishi, T. (1987) EPR characterization of the iron-sulfur clusters in the NADH: Ubiquinone oxidoreductase segment of the respiratory chain in Paracoccus denitrificans. *J. Biol. Chem. 262*, 9147–9153.

6. Leif, H., Sled, V. D., Ohnishi, T., Weiss, H., and Friedrich, T. (1995) Isolation and characterization of the proton-translocating NADH: Ubiquinone oxidoreductase from *Escherichia coli*. *Eur. J. Biochem. 230*, 538–548.
7. Yano, T., Sklar, J., Nakamaru-Ogiso, E., Takahashi, Y., Yagi, T., and Ohnishi, T. (2003) Characterization of cluster N5 as a fast-relaxing [4Fe-4S] cluster in the Nqo3 subunit of the proton-translocating NADH-ubiquinone oxidoreductase from *Paracoccus denitrificans*. *J. Biol. Chem. 278*, 15514–15522.
8. Zu, Y., Di Bernardo, S., Yagi, T., and Hirst, J. (2002) Redox properties of the [2Fe-2S] center in the 24 kDa (NQO2) subunit of NADH:ubiquinone oxidoreductase (complex I). *Biochemistry 41*, 10056–10069.
9. Ohnishi, T. (1998) Iron-sulfur clusters/semiquinones in complex I. *Biochim. Biophys. Acta 1364*, 186–206.
10. Hirst, J. (2005) Energy transduction by respiratory complex I—An evaluation of current knowledge. *Biochem. Soc. Trans. 33*, 525–529.
11. Krishnamoorthy, G., and Hinkle, P. C. (1988) Studies on the electron transfer pathway, topography of iron-sulfur centers, and site of coupling in NADH-Q oxidoreductase. *J. Biol. Chem. 263*, 17566–17575.
12. Sazanov, L. A., and Hinchliffe, P. (2006) Structure of the hydrophilic domain of respiratory complex I from *Thermus thermophilus*. *Science 311*, 1430–1436.
13. Calhoun, M. W., and Gennis, R. B. (1993) Demonstration of separate genetic-loci encoding distinct membrane-bound respiratory NADH dehydrogenases in *Escherichia coli*. *J. Bacteriol. 175*, 3013–3019.
14. Sinegina, L., Wikström, M., Verkhovsky, M. I., and Verkhovskaya, M. L. (2005) Activation of isolated NADH:ubiquinone reductase I (complex I) from *Escherichia coli* by detergent and phospholipids. Recovery of ubiquinone reductase activity and changes in EPR signals of iron-sulfur clusters. *Biochemistry 44*, 8500–8506.
15. Belevich, G., Euro, L., Wikström, M., and Verkhovskaya, M. (2007) Role of the conserved arginine 274 and histidine 224 and 228 residues in the NuoCD subunit of complex I from *Escherichia coli*. *Biochemistry 46*, 526–533.
16. Harder, S. R., Feinberg, B. A., and Ragsdale, S. W. (1989) A spectroelectrochemical cell designed for low temperature electron paramagnetic resonance titration of oxygen-sensitive proteins. *Anal. Biochem. 181*, 283–287.
17. Harder, S. R., Lu, W. P., Feinberg, B. A., and Ragsdale, S. W. (1989) Spectroelectrochemical studies of the corrinoid/iron-sulfur protein involved in acetyl coenzyme A synthesis by *Clostridium thermoaceticum*. *Biochemistry 28*, 9080–9087.
18. Bogachev, A. V., Bertsova, Y. V., Bloch, D. A., and Verkhovsky, M. I. (2006) Thermodynamic properties of the redox centers of Na(+)-translocating NADH:quinone oxidoreductase. *Biochemistry 45*, 3421–3428.
19. Massey, V., and Palmer, G. (1962) Charge transfer complexes of lipoyl dehydrogenase and free flavins. *J. Biol. Chem. 237*, 2347–2358.
20. Stankovich, M. T., Schopfer, L. M., and Massey, V. (1978) Determination of glucose oxidase oxidation-reduction potentials and the oxygen reactivity of fully reduced and semiquinoid forms. *J. Biol. Chem. 253*, 4971–4979.
21. Fu, W., Jack, R. F., Morgan, T. V., Dean, D. R., and Johnson, M. K. (1994) nifU gene product from *Azotobacter vinelandii* is a homodimer that contains two identical [2Fe-2S] clusters. *Biochemistry 33*, 13455–13463.
22. Mayhew, S. G., Petering, D., Palmer, G., and Foust, G. P. (1969) Spectrophotometric titration of ferredoxins and chromatium high potential iron protein with sodium dithionite. *J. Biol. Chem. 244*, 2830–2834.
23. Yano, T., Sled′, V. D., Ohnishi, T., and Yagi, T. (1996) Expression and characterization of the flavoprotein subcomplex composed of 50-kDa (NQO1) and 25-kDa (NQO2) subunits of the proton-translocating NADH-quinone oxidoreductase of *Paracoccus denitrificans*. *J. Biol. Chem. 271*, 5907–5913.
24. Velazquez, I., Nakamaru-Ogiso, E., Yano, T., Ohnishi, T., and Yagi, T. (2005) Amino acid residues associated with cluster N3 in the NuoF subunit of the proton-translocating NADH-quinone oxidoreductase from *Escherichia coli*. *FEBS Lett. 579*, 3164–3168.
25. Yakovlev, G., Reda, T., and Hirst, J. (2007) Reevaluating the relationship between EPR spectra and enzyme structure for the iron sulfur clusters in NADH:quinone oxidoreductase. *Proc. Natl. Acad. Sci. U.S.A. 104*, 12720–12725.
26. Barker, C. D., Reda, T., and Hirst, J. (2007) The flavoprotein subcomplex of complex I (NADH:ubiquinone oxidoreductase) from bovine heart mitochondria: Insights into the mechanisms of NADH oxidation and NAD+ reduction from protein film voltammetry. *Biochemistry 46*, 3454–3464.
27. Nakamaru-Ogiso, E., Yano, T., Yagi, T., and Ohnishi, T. (2005) Characterization of the iron-sulfur cluster N7 (N1c) in the subunit NuoG of the proton-translocating NADH-quinone oxidoreductase from *Escherichia coli*. *J. Biol. Chem. 280*, 301–307.
28. Pohl, T., Bauer, T., Dorner, K., Stolpe, S., Sell, P., Zocher, G., and Friedrich, T. (2007) Iron-sulfur cluster N7 of the NADH: ubiquinone oxidoreductase (complex I) is essential for stability but not involved in electron transfer. *Biochemistry 46*, 6588–6596.
29. Ohnishi, T., Blum, H., Galante, Y. M., and Hatefi, Y. (1981) Iron-sulfur N-1 clusters studied in NADH-ubiquinone oxidoreductase and in soluble NADH dehydrogenase. *J. Biol. Chem. 256*, 9216–9220.
30. Laurents, D. V., Huyghues-Despointes, B. M., Bruix, M., Thurlkill, R. L., Schell, D., Newsom, S., Grimsley, G. R., Shaw, K. L., Trevino, S., Rico, M., Briggs, J. M., Antosiewicz, J. M., Scholtz, J. M., and Pace, C. N. (2003) Charge-charge interactions are key determinants of the pK values of ionizable groups in ribonuclease Sa (pI = 3.5) and a basic variant (pI = 10.2). *J. Mol. Biol. 325*, 1077–1092.
31. Schutz, C. N., and Warshel, A. (2001) What are the dielectric "constants" of proteins and how to validate electrostatic models? *Proteins 44*, 400–417.
32. Albracht, S. P., Dooijewaard, G., Leeuwerik, F. J., and Swol, B. V. (1977) EPR signals of NADH: Q oxidoreductase. Shape and intensity. *Biochim. Biophys. Acta 459*, 300–317.
33. Grgic, L., Zwicker, K., Kashani-Poor, N., Kerscher, S., and Brandt, U. (2004) Functional significance of conserved histidines and arginines in the 49-kDa subunit of mitochondrial complex I. *J. Biol. Chem. 279*, 21193–21199.

BI702063T